

Conf-9406246--2

UCRL-JC-116992
PREPRINT

Solid Hydrogen Structure

G. W. Collins
W. G. Unites
E. R. Mapoles
F. Magnotta
T. P. Bernat

This paper was prepared for submittal to the
Conference Proceedings for the 1994 Air Force
HDEM Contractor's Conference
Crystal Bay, NV
June 5-7, 1994

November 1994

RECEIVED

JUL 18 1995

OSTI



Lawrence
Livermore
National
Laboratory

This is a preprint of a paper intended for publication in a journal or proceedings. Since changes may be made before publication, this preprint is made available with the understanding that it will not be cited or reproduced without the permission of the author.

DISCLAIMER

This document was prepared as an account of work sponsored by an agency of the United States Government. Neither the United States Government nor the University of California nor any of their employees, makes any warranty, express or implied, or assumes any legal liability or responsibility for the accuracy, completeness, or usefulness of any information, apparatus, product, or process disclosed, or represents that its use would not infringe privately owned rights. Reference herein to any specific commercial product, process, or service by trade name, trademark, manufacturer, or otherwise, does not necessarily constitute or imply its endorsement, recommendation, or favoring by the United States Government or the University of California. The views and opinions of authors expressed herein do not necessarily state or reflect those of the United States Government or the University of California, and shall not be used for advertising or product endorsement purposes.

DISCLAIMER

Portions of this document may be illegible in electronic image products. Images are produced from the best available original document.

Solid hydrogen structure

G. W. Collins, W. G. Unites, E. R. Mapoles, F. Magnotta, and T. P. Bernat
Lawrence Livermore National Laboratory, Livermore, CA 94551

ABSTRACT

The $J=0 \rightarrow 2$ Raman signal from solid $J=0$ D_2 or H_2 reveals HCP structure when deposited at a rate $0.1 \leq R(\mu\text{m}/\text{min}) \leq 40$ onto MgF_2 at $T_d/T_{tp} > 0.3$, a mixture of HCP and FCC crystals at $0.2 < T_d/T_{tp} < 0.3$ and possibly a randomly stacked close packed structure at $T_d/T_{tp} < 0.2$, where T_{tp} is the triple point temperature. Non-HCP crystals transform to HCP continuously and irreversibly with increasing T . Finally, the crystal size decreases with decreasing T_d and increasing R , from ~ 1 mm at $T_d \sim 0.8 T_{tp}$ and $R \sim 2 \mu\text{m}/\text{min}$ to $\sim 1 \mu\text{m}$ at $0.25 T_{tp}$ and $R \sim 40 \mu\text{m}/\text{min}$.

INTRODUCTION

Near the triple point temperature, T_{tp} , hydrogen typically forms an hexagonal close packed (HCP) structure.^{1,2,3} Since the interaction between hydrogen molecules is weak, the rotational quantum number is well defined in the low pressure solid at temperatures above $0.2 T_{tp}$, and most of the molecules are either in the ground ($J=0$) or first excited ($J=1$) rotational state. When cooled to a low enough temperature with a large enough $J=1$ concentration, $[J=1] > 55\%$, the lattice transforms from HCP to face centered cubic (FCC) with the molecules ordered to form Pa_3 symmetry. This phase transition lowers the electric quadrupole-quadrupole (EQQ) energy for $J=1$ molecules by about 5 K/molecule, which is much greater than the ~ 1 mK/molecule energy difference between HCP and FCC structures. However, when all of the molecules are in the $J=0$ state, the equilibrium crystal structure at all temperatures and pressures below ~ 100 GPa is HCP.⁴ Nature chooses this equilibrium lattice structure because it has the lowest Gibbs free energy, but this free energy difference between HCP and FCC $J=0$ hydrogen is not well understood.

Crystal structures other than HCP have been observed for solid $J=0$ hydrogen under some conditions. First, thin hydrogen films grown from the vapor or liquid can take on the underlying lattice structure of the substrate.

Second, thin ($\sim 10\text{nm}$) hydrogen films deposited at temperatures below $\sim 0.4 T_{\text{tp}}$ can be grown with an FCC lattice structure.^{5,6} When heated, these layers exhibited sharp electron diffraction peaks indicating an HCP structure. These observations imply that HCP is the equilibrium crystal form at high temperature, while for thin films the FCC phase may be stable or metastable at low temperatures.

Rare gas solids also form simple molecular solids with lattice potentials similar to hydrogen. However, the heavier rare gas solids, Ne, Ar, Kr, and Xe, all crystallize into FCC at low pressure, while the lightest rare gas, ^4He , primarily forms HCP structure at low temperature and pressure, and FCC only at high temperature and pressure. Most two-body potentials, summed over all neighbors, yield a slightly lower energy for HCP rather than FCC structures; thus, the FCC lattice in the heavy rare gases is thought to be due to the dispersion interaction between nearest neighbors.⁷ The HCP structure forms in ^4He and possibly $J=0$ hydrogen because the dispersion interaction for the closed shell S state orbital is comparatively small.

In this paper we investigate the lattice structure and crystal morphology of thick ($>10\ \mu\text{m}$) H_2 and D_2 layers grown from the gas phase at deposition rates, $0.1 < R(\mu\text{m}/\text{min}) < 40$ and deposition temperatures $3.5\ \text{K} < T_{\text{d}} < 11\ \text{K}$. As discussed below, we observe a triplet for the $J=0 \rightarrow 2$ Raman signal of solid $J=0\ \text{H}_2$ or $J=0\ \text{D}_2$ deposited on MgF_2 ⁸ when $T_{\text{d}}/T_{\text{tp}} > 0.3$ where the triple point temperatures are $T_{\text{tp}}(J=0\ \text{H}_2) = 13.8\ \text{K}$ and $T_{\text{tp}}(J=0\ \text{D}_2) = 18.7\ \text{K}$.⁹ Van Kranendonk has shown this triplet to be a unique signature of HCP structure.¹⁰ At $0.2 < T_{\text{d}}/T_{\text{tp}} < 0.3$ we resolve four narrow peaks for this Raman transition which we show is due to a mixture of HCP and FCC crystallites which appears at $T_{\text{d}}/T_{\text{tp}} \sim 0.3$, and increases with decreasing T_{d} . As $T_{\text{d}}/T_{\text{tp}}$ decreases below 0.2 in $J=0\ \text{D}_2$, the same Raman signal transforms from a resolved quadruplet into an unresolved signal consisting of two main branches. This transformation may indicate a new structure with less symmetry such as a randomly stacked close packed lattice. The two and four-peak multiplets transform continuously and irreversibly into a triplet upon increasing the temperature through $T/T_{\text{tp}} \sim 0.5$. We also observe that co-depositing N_2 in $J=0\ \text{D}_2$ at $5.5\ \text{K}$ ($\sim 0.3 T_{\text{tp}}$) forms the four-peak multiplet at concentrations near $[\text{N}_2] \sim 0.05\%$ and the unresolved doublet for $[\text{N}_2] \sim 0.5\%$. Furthermore, the addition of N_2 inhibits the transformation to HCP upon increasing T . Finally, photographic techniques show the size of H_2 or D_2

crystallites decreases with decreasing T_d and increasing R , from millimeter scale at $T_d \sim 0.8 T_{tp}$ and $R \sim 2 \mu\text{m}/\text{min}$ to micron scale at $T_d \sim 0.3 T_{tp}$ and $R \sim 40 \mu\text{m}/\text{min}$.

EXPERIMENTAL DETAILS

The experimental details will be described more completely in a later publication.¹¹ Briefly, the sample cell is made of copper and fitted with two opposing sapphire windows so that light can pass directly through the cell. The windows are attached with crushed indium seals for thermal contact, vertically mounted, and serve as the sample substrate while permitting optical access to the hydrogen crystals. The cell is connected to the cold tip of a helium flow cryostat. Both the radiation shield operating at a temperature of 30 K and the room temperature vacuum jacket enclosing the sample cell, contain sapphire windows for optical access. A calibrated germanium resistance thermometer is fitted on the copper sample cell. The absolute thermometer temperature on the sapphire window is set by the triple point of D_2 and H_2 . At temperatures above $\sim 0.5 T_{tp}$, we compare the thermometer temperature with the temperature calculated from the hydrogen vapor pressure. The vapor pressure is measured by a capacitance manometer and converted to temperature using the equation of state.¹² The agreement between the vapor pressure temperature and the germanium thermometer temperature determines the accuracy of the temperature measurement to be better than 0.05 K.

The H_2 and D_2 gas were high purity research grade with an isotopic purity of 99.9% and 99.8% respectively. The samples studied here contained a $J=1$ concentration less than 1%. The rotational and isotopic concentration is determined by comparing the Raman line intensities for the $J=0 \rightarrow 2$ and $J=1 \rightarrow 3$ transitions. The hydrogen gas was cooled to $\sim 20 - 30$ K just before deposition. The deposition rates are determined by measuring the layer thickness as a function of time by interferometric techniques. All the samples studied here were between $10 \mu\text{m}$ and $300 \mu\text{m}$ thick.

We measured the Raman shift of the 488 nm line of an Ar ion Laser in back scattering geometry with a modified 1/2 meter SPEX 1870 spectrograph fitted with a liquid nitrogen cooled CCD having a $22.5 \mu\text{m}$ pixel width. Our spectral resolution was $\sim 0.4 \text{ cm}^{-1}$. To determine the line positions we used both a calibrated thorium lamp and the triplet structure of H_2 or D_2

crystallized through the triple point and their line positions as measured by Bhatnagar et al.¹⁵ The laser power level ($\sim 10 - 100$ mW) was set so as to not influence the lattice structure or visually change the layer morphology.

EXPERIMENTAL DATA AND DISCUSSION

Figure 1a shows the triplet for the $J=0 \rightarrow 2$ rotational Raman signal for H_2 deposited at 5.5 K and ~ 5 $\mu\text{m}/\text{min}$. Fig. 1b, 1d and 1e show the same Raman transition in H_2 deposited at 3.5 K and 2 $\mu\text{m}/\text{min}$, D_2 at 3.5 K and 0.2 $\mu\text{m}/\text{min}$, and D_2 at 5.2 K and 0.4 $\mu\text{m}/\text{min}$. The four peaks shown in Fig. 1b and 1e are common for $3.5 \text{ K} \leq T_d(H_2) < 4 \text{ K}$ and $4 < T_d(D_2) \leq 6$ and deposition rates between $0.1 < R(\mu\text{m}/\text{min}) < 40$. The spectrum shown in Fig. 1d is typical for $3.5 \leq T_d(D_2) < 4 \text{ K}$ where it appears the peaks in Fig. 1e shift towards an unresolved lineshape with two main branches. Figure 1c (1f) shows the same transition for the H_2 (D_2) sample in Fig. 1b (Fig. 1e) a couple minutes after rapidly warming from 3.5 K (5.2 K) to 7 K (11.4 K). We find the quadruplet shown in Fig. 1b and 1e and the unresolved "doublet" shown in Fig. 1d transform to a triplet within minutes upon warming the sample rapidly through $\sim 0.5 T_{tp}$. At constant temperature the Raman spectra shown in Fig. 1 are stable for at least two days, the maximum duration of observation.

Figure 2a shows the temperature dependence of the $J=0 \rightarrow 2$ Raman spectrum, upon warming solid $J=0$ D_2 , deposited at 5.3 K and 2.2 $\mu\text{m}/\text{min}$. We see a steady decrease in the relative intensity of the first and fourth peak with increasing temperature. This transformation is not reversible; when the temperature is decreased at any point during this experiment, the relative first and fourth peak heights do not increase back. Figure 2a also shows a slight shift in the spectrum of $\sim -0.45 \text{ cm}^{-1}$ upon warming from 5 to 7 K. The high energy peak may be shifted slightly more (~ -0.70 to -0.90 cm^{-1}) than the other low energy peaks. The quadruplet Raman signal in H_2 transforms to a triplet upon slowly raising T to $\sim 5.5 \text{ K}$. We saw no shift in the H_2 Raman spectrum upon warming from 3.5 to 7 K.

Figure 2b shows the time dependence of the transformation shown in Fig. 2a by plotting both the sample cell temperature and the intensity of the low energy Raman peak divided by the average of the other three peaks, $R_{\text{FCC/HCP}}$, versus time. The rationale for using this ratio is explained later. In several other experiments we have deposited D_2 between 5.1 K and 5.5 K and

held the sample at constant temperature for ~ 2 days without a noticeable change in $R_{\text{FCC/HCP}}$. These data show $R_{\text{FCC/HCP}}$ is roughly constant at constant temperature, decreases with increasing temperature, and evolves to steady state over the period of several minutes. In Fig. 2c we plot $R_{\text{FCC/HCP}}$ vs temperature (all values, not just the steady state value) from 3 different experiments. The large scatter of points at each temperature is primarily due to the time dependence at constant temperature shown in Fig. 2b. The plot is approximately linear from 6 K to 11 K.

The unresolved broad doublet shown in Fig. 1d shows a different behavior with increasing temperature than the four peak spectra. Upon increasing T from $T_d \sim 3.5$ K to 7 K the two overlapping lines in the right hand branch of the spectrum separated slightly but the general structure of the spectrum still consisted of 2 main branches. Upon increasing T to ~ 10 K, the structure transformed into a well resolved triplet similar to that shown in Fig. 1f, within ~ 10 minutes. Figure 3 shows the effect of co-depositing N_2 with $J=0$ D_2 on the $J=0 \rightarrow 2$ Raman spectrum. Figure 3a (3b) shows the rotational Raman spectrum for $\text{D}_2 + 0.05\% \text{N}_2$ ($\text{D}_2 + 0.5\% \text{N}_2$) deposited at $R=2 \mu\text{m}/\text{min}$ and at $T = T_d = 5.5$ K. Fig. 3a shows $0.05\% \text{N}_2$ in D_2 affects the $J=0 \rightarrow 2$ Raman transition only slightly. The open circles in Fig. 2c show the temperature dependence of $R_{\text{FCC/HCP}}$ for this $\text{D}_2 + 0.05\% \text{N}_2$ sample revealing a slightly larger value at all temperatures than pure D_2 . The first three points were taken 1 hr apart and decreased with time at the constant temperature of 5.5 K to $R_{\text{FCC/HCP}} \sim 0.6$. The sample warmed up slowly over the next 12 hours to 8.6 K. The rest of the data were taken allowing the sample to relax for ~ 10 minutes after the temperature increase. We see from Fig. 3b ($\text{D}_2 + 0.5\% \text{N}_2$) that the broad unresolved signal similar to Fig. 1d is formed at a higher temperature than 4 K for pure D_2 . Furthermore, this broad signal was stable up to ~ 17 K for several minutes.¹³

What do the different Raman spectra discussed above mean? Van Kranendonk has proved that the triplet signals shown in Fig. 1 are unique signatures of HCP symmetry.¹⁴ FCC symmetry produces a doublet with a splitting of $\sim 7 \text{ cm}^{-1}$ in H_2 and 9 cm^{-1} in D_2 . The $J=0 \rightarrow 2$ Raman shift containing the first order crystal field interaction is calculated to be 354 cm^{-1} and 179 cm^{-1} for $J=0$ H_2 and D_2 respectively. When the electric quadrupole-quadrupole interaction is taken into account, Raman accessible energy eigenvalues split from the zeroth order values. Using the expressions from

Van Kranendonk we calculate for an HCP lattice, $\Delta E(m_J) = 2.98 \text{ cm}^{-1}$, -1.99 cm^{-1} , 0.5 cm^{-1} for $m_J = 0, 1, 2$ for H_2 and $\Delta E(m_J) = 3.68 \text{ cm}^{-1}$, -2.46 cm^{-1} , 0.61 cm^{-1} for $m_J = 0, 1, 2$ for D_2 . For an FCC lattice, $\Delta E_1 = -4.38 \text{ cm}^{-1}$, and $\Delta E_2 = 2.92 \text{ cm}^{-1}$ for H_2 and $\Delta E_1 = -5.43 \text{ cm}^{-1}$, $\Delta E_2 = 3.62 \text{ cm}^{-1}$ for D_2 . The calculated values for the HCP lattice are close to the measured values of Bhatnagar et al.¹⁵ who find peaks at 351.84 cm^{-1} , 353.85 cm^{-1} , and 355.83 cm^{-1} for $J=0 \text{ H}_2$ and 176.8 cm^{-1} , 179.4 cm^{-1} , and 182.0 cm^{-1} for $J=0 \text{ D}_2$.

The peak positions we find for the H_2 triplet in Fig 1a and 1c are at 352 cm^{-1} , 354 cm^{-1} , and 356 cm^{-1} ; the H_2 quadruplet in Fig. 1b are at $\sim 350 \text{ cm}^{-1}$, 352 cm^{-1} , 354 cm^{-1} , and 356 cm^{-1} ; the D_2 triplet in Fig. 1f are at 177 cm^{-1} , 179 cm^{-1} , and 182 cm^{-1} ; the D_2 quadruplet in Fig. 1e are at 175 cm^{-1} , 177 cm^{-1} , 179 cm^{-1} , and 182 cm^{-1} . The calculated and measured spectra show the lattice is a mixture of FCC and HCP structure.¹⁶ The individual lines in Fig. 1b and Fig. 1e are narrow and well separated as compared to the lineshape shown in Fig. 1d. We speculate that the samples giving rise to the narrow line resolved spectra are small crystallites with FCC or HCP structure and the unresolved lineshape indicates a lattice structure with less symmetry, such as a randomly stacked close packed lattice. The unresolved lineshape is probably not resulting from an amorphous structure since an amorphous phase should give rise to a single broad line similar to that found in the liquid phase.

Thus as T_d decreases between $0.2 < T_d/T_{tp} < 0.3$ the relative intensity of the low and high energy peaks increase. After deposition, as T is increased towards $0.5 T_{tp}$, the low and high energy peaks decrease. This is expected if an FCC component occurs at $T_d/T_{tp} < 0.3$ and increases with decreasing T_d . This is why we defined the ratio $R_{\text{FCC/HCP}}$ which is a relative measure of FCC to HCP structure in the sample. The irreversible decrease in $R_{\text{FCC/HCP}}$ with increasing temperature suggests the FCC component, once formed, is metastable at $T < 0.5 T_{tp}$. The equilibration of $R_{\text{FCC/HCP}}$ after each temperature increase suggests the FCC phase is separated from the lower energy HCP phase by many different barrier energies. Since the outside peaks of the lineshape from N_2 doped D_2 , shown in Fig. 3, are relatively larger than the corresponding lineshapes in pure D_2 , shown in Fig. 1, we conclude that codepositing N_2 with hydrogen increases the fraction of FCC structure.

At constant T_d we also see a slight increase in the FCC component with decreasing R . This implies that the FCC component may be found at

$T_d/T_{tp} > 0.3$ if we deposited at lower R . This effect may be due to sample heating.

While the relative temperature for structural change in H_2 and D_2 is similar, it is not the same. The temperature at which the mixed FCC + HCP structure transforms to pure HCP is relatively lower in H_2 (~ 5.5 K) than in D_2 (~ 10.5 K). Thus the HCP phase is more stable in H_2 than in D_2 . If the FCC phase is metastable and separated from the HCP phase by many different energy barriers, and if tunneling is a dominant mechanism for molecular motion at these low temperatures, then H_2 would be able to cross the energy barriers to reach the lower energy HCP phase more rapidly than D_2 . Although tunneling diffusion has been observed for hydrogen atoms in solid hydrogen,¹⁷ tunneling of molecules in solid hydrogen has not been clearly observed.¹⁸

For the back-scattering geometry used here, we define the incident and scattered wave vector to be along X , the incident electric field polarization vector along Y , and the scattered polarization vector is along Z . We use F/3 optics to couple light in and out of the sample, but for our calculation we will assume that the light is collimated. The relative intensity ratio for the triplet signals in Fig. 1 imply there is a preferential crystallite alignment with the c axes along the direction of the laser and thus perpendicular to the substrate. The relative $m_j = 1, 2, 0$ intensity ratios for Fig. 1a, Fig. 1c and Fig. 1f are 0.33:1:0.15, 0.55:1:0.21, and 0.64:1:0.34. For a powder average of HCP crystallites the ratio should be 1:1:0.5 while for the c axis perpendicular to the substrate we expect 0:1:0. Although a preferential growth along the c -axis has been observed near the triple point, it is a bit confusing why these small crystals would grow in a preferred direction or transform from FCC to HCP in a preferred orientation.

We next describe the appearance of layers under low temperature vapor deposition conditions. Figure 4a, 4b, and 4c show shadowgraph images of H_2 deposited at $R = 40 \mu\text{m}/\text{min}$ and $T_d = 3.6 \text{ K}, 7.0 \text{ K},$ and 11 K . These and similar experiments qualitatively show the average crystal size decreases rapidly with decreasing temperature and increasing deposition rate between $3.6 < T_d < 11 \text{ K}$ and $0.1 < R(\mu\text{m}/\text{min}) < 40$. Figure 5 shows the change in the average crystal diameter versus temperature at different deposition rates. The smallest crystal diameter is at the limit of our optical resolution ~ $3 \mu\text{m}$ and is thus a very rough estimate.¹⁹

Since the deposition temperatures used here are below the roughening transition temperatures for the low energy crystal facets,²⁰ the lowest free energy configuration is in the form of faceted microcrystals. The appearance of smooth rounded crystallites as in Fig. 4b implies the crystal morphology is non-equilibrium and is determined by kinetics. To qualitatively understand the dependence of crystal size on temperature and deposition rate, we assume the temperature controls the rate at which molecules relax from a high energy to low energy configuration. We expect the lowest energy site to be that with the maximum number of neighboring bonds such as a step edge of a crystal. As the temperature decreases and/or the deposition rate increases the probability of finding a low energy site before the next layer of material covers the substrate decreases.

In conclusion, the structural phase transition reported here may elucidate recent experiments where low temperature deposition of hydrogen was used to trap atomic impurities,²¹ or to form a weakly interacting Van der Waals substrates to study surface state electron mobility^{22,23,24,25} and phase transitions of helium films.²⁶ D atoms in solid deuterium films deposited from the gas phase at ~ 3 K have a significantly different activation energy than expected for the equilibrium HCP structure.¹⁸ In the surface state electron mobility experiments, solid hydrogen films grown at 1.5 K and containing surface electrons have a conductivity less than 10^{-11} mho at a temperature between 2 and 3.5 K on just deposited films. After annealing at 4.2 K the conductivity increases to, $\sigma \sim 10^{-9}$ mho at 2 K with an activation energy of ~ 18 K. After annealing the hydrogen layer at ~ 8 K, the conductivity increases to, $\sigma \sim 10^{-8}$ mho with an activation energy of ~ 10 K. The nonequilibrium structure described in this paper and analogous lower temperature structures may be the important factor controlling the mobility of electrons, atoms, and molecules in these low temperature deposited hydrogen films.

We gratefully acknowledge partial financial support of the Air Force High Energy Density Materials Program at the Phillips Laboratory. This work was performed under the auspices of the U. S. Department of Energy by the Lawrence Livermore National Laboratory under Contract No. W-7405-ENG-48.

- ¹Isaac F. Silvera, *Rev. Mod. Phys.* **52**, 393 (1980).
- ²P. C. Souers, *Hydrogen Properties for Fusion Energy* (University of California, Berkeley, 1986), Chapter 6.
- ³Thin films can take on the underlying lattice structure of the substrate. C. S. Barrett, L. Meyer, and J. Wasserman, *J. Chem. Phys.* **45**, 834 (1966).
- ⁴Jan Van Kranendonk, *Solid Hydrogen* (Plenum Press, New York, 1983), p. 226.
- ⁵O. Bostanjoglo, and R. Kleinschmidt, *J. Chem. Phys.* **46**, 2004 (1967).
- ⁶A. E. Curzon and A. J. Mascall, *Brit. J. Appl. Phys.* **16**, 1301 (1965).
- ⁷K. F. Niebles and J. A. Venables in *Rare Gas Solids*, Vol. 1, ed. by M. L. Klein and J. A. Venables, (Academic Press, New York, 1976), Chapter 9.
- ⁸The MgF₂ was an amorphous or nanocrystalline 1/4 wave thick (at 550 nm) antireflectance thin film, vapor deposited onto a sapphire window which was cleaved normal to the c-axis. The MgF₂ film was prepared by Meller Optics Co.
- ⁹Reference 2, p. 80.
- ¹⁰Reference 4, Chapter 4.
- ¹¹G. W. Collins, E. R. Mapoles, T. P. Bernat, and W. G. Unites, *Solid Hydrogen Films*, in preparation.
- ¹²Reference 2, p. 49.
- ¹³After melting the D₂+0.5%N₂ sample, N₂ plated on the windows; then when a thin film of D₂ was frozen near the triple point onto the N₂, there were only two narrow peaks in the J=0→2 Raman spectrum at 175 cm⁻¹ and 182 cm⁻¹.
- ¹⁴Reference 4, p. 114.
- ¹⁵S. S. Bhatnagar, E. J. Allin, and H. L. Welsh, *Can. J. Phys.* **40**, 9 (1962).
- ¹⁶We do not believe the FCC component is influenced by nanocrystalline structure of the MgF₂ substrate because the crystals forming at T_d > 0.3T_{tp} are HCP, and at T_d < 0.3T_{tp}, hydrogen crystallites are small (<50μm) and decreasing in size with decreasing temperature.
- ¹⁷G. W. Collins, P. C. Souers, J. L. Maienschein, E. R. Mapoles and J. R. Gaines, *Phys. Rev. B* **45**, 549 (1992). A. V. Ivliev, A. Ya. Katunin, I. I. Lukashevich, V. V. Sklyarevskii, V. V. Suraev, V. V. Filippov, N. I. Filippov and V. A. Shevtsov, *JETP Lett.* **36**, 472 (1982). A. S. Iskovskikh, A. Ya. Katunin, I. I. Lukashevich, V. V. Sklyarevskii, V. V. Suraev, V. V. Filippov, N. I. Filippov and V. A. Shevtsov, *Sov. Phys. JETP* **64**, 1085 (1986).
- ¹⁸J. R. Gaines, P. A. Fedders, G. W. Collins, J. D. Sater, and P. C. Souers, "Diffusion in the solid hydrogens," submitted to *Phys. Rev. B*.
- ¹⁹Crystals left at constant temperature, even near 3.5 K, appeared to increase slightly with time, although we did not study this phenomena in detail.
- ²⁰G. W. Collins, E. R. Mapoles, T. P. Bernat, and W. G. Unites, *Roughening Transition in Solid Deuterium*, in preparation.
- ²¹A. V. Ivliev, A. S. Iskovskikh, A. Ya. Katunin, I. I. Lukashevich, V. V. Sklyarevskii, V. V. Suraev, V. V. Filippov, N. I. Filippov, and V. A. Shevtsov, *JETP Lett.* **38**, 379 (1983); E. B. Gordon, A. A. Pelmenev, O. F. Pugachev and V. V. Khmelenko, *JETP Lett.* **37**, 282 (1983).
- ²²M. A. Paalanen and Y. Iye, *Surface Science*, **170**, 80 (1986).
- ²³K. Kono, U. Albrecht, and P. Leiderer, *J. Low Temp. Physics*, **82**, 279 (1991).
- ²⁴M. A. Paalanen and Y. Iye, *Surface Science*, **170**, 80 (1986).
- ²⁵U. Albrecht, H. Dilger, P. Leiderer, and K. Kono, *Physica B*, **165-166**, 841 (1990).
- ²⁶John G. Brisson, John C. Mester, and Isaac F. Silvera, *Phys. Rev. B* **44**, 12453 (1991).

FIGURES

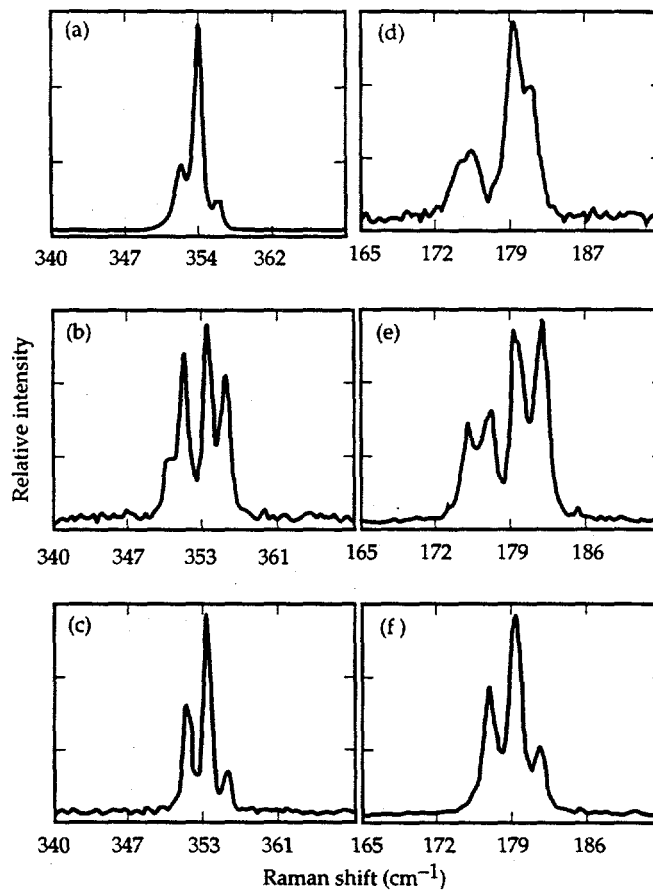


FIG. 1 $J=0$ to 2 Raman signal for (a) H_2 deposited at 5.5 K and $5 \mu\text{m}/\text{min}$, (b) H_2 deposited at 3.5 K and $2 \mu\text{m}/\text{min}$, (c) same sample as Fig. 1b after warming from 3.5 K to 7 K, (d) D_2 deposited at 3.5 K and $0.2 \mu\text{m}/\text{min}$, (e) D_2 deposited at 5.2 K and $0.4 \mu\text{m}/\text{min}$, (f) same sample as Fig. 1e after warming from 5.2 K to 11.4 K.

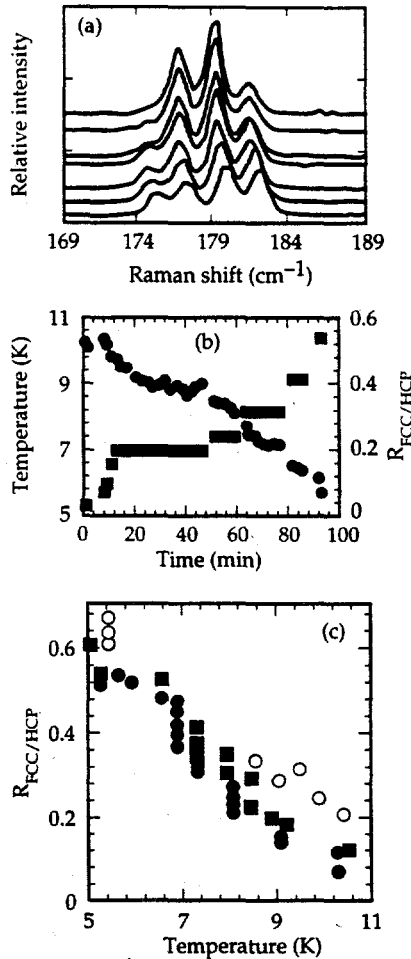


FIG. 2 Temperature and time dependence of the $J=0 \rightarrow 2$ Raman spectrum, upon warming solid $J=0$ D_2 . (a) The sample was deposited at 5.3 K and $2.2 \mu\text{m}/\text{min}$; From bottom to top (i) the resultant spectra after deposition at 5.3 K, (ii) after raising the temperature to 6.9 K, (iii) after waiting at 6.9 K for 34 minutes, (iv) after raising the temperature to 7.4 K and waiting 8 minutes, (v) after 13 minutes at 8.1 K, (vi) after 5 minutes at 9.1 K, and (vii) after 2 minutes at 10.4K. (b) Time dependence of the phase transformation shown in Fig. 2a. Dark circles are the height ratio of the low energy Raman peak divided by the average of the other three peaks ($R_{\text{FCC}/\text{HCP}}$): Dark squares show the temperature of the sample. (c) $R_{\text{FCC}/\text{HCP}}$ versus temperature from 3 different experiments. The dark circles show the same experiment as in Fig. 2a and 2b. Dark squares show a similar experiment with $J=0$ D_2 deposited at 5.1 K and $0.4 \mu\text{m}/\text{min}$. After deposition the sample sat at ~ 5.3 K for 23 hrs and then we began raising the temperature at about 0.5 K/20 min. Open circles show $J=0$ $D_2 + 0.05\%$ N_2 deposited at 5.5 K and $2 \mu\text{m}/\text{min}$.

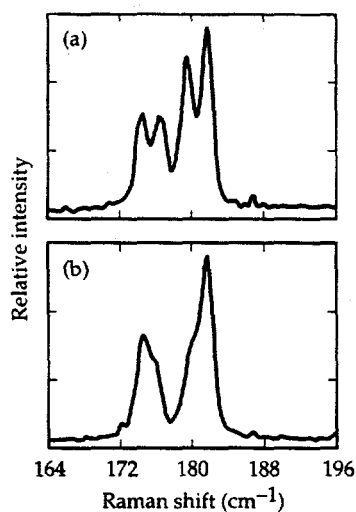


FIG. 3 $J=0 \rightarrow 2$ Raman spectra for (a) $J=0$ $D_2 + 0.05\%$ N_2 deposited at 5.5 K and $2 \mu\text{m}/\text{min}$, and (b) $J=0$ $D_2 + 0.5\%$ N_2 deposited at 5.5 K and $2 \mu\text{m}/\text{min}$.

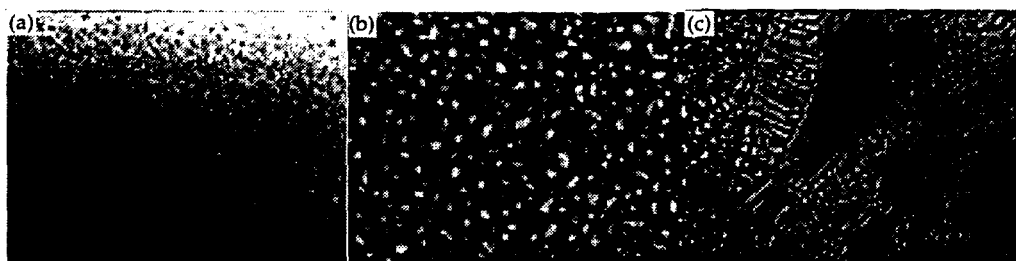


FIG. 4 Shadowgraph images for H_2 deposited at $40 \mu\text{m}/\text{min}$ and (a) 3.6 K, (b) 7.0 K, and (c) 11 K. The horizontal field of view is 1.7 mm.

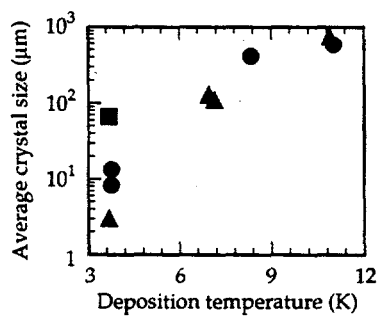


FIG. 5 Average crystallite size versus deposition temperature for H_2 deposited at $0.2 \mu\text{m}/\text{min}$ (dark squares), $2 \mu\text{m}/\text{min}$ (dark circles), and $40 \mu\text{m}/\text{min}$ (dark triangles).